

This discussion paper is/has been under review for the journal Natural Hazards and Earth System Sciences (NHESD). Please refer to the corresponding final paper in NHESD if available.

Importance of three-dimensional grids and time-dependent factors for the applications of earthquake forecasting models to subduction environments

C.-H. Chan

Earth Observatory of Singapore, Nanyang Technological University, Singapore, Singapore

Received: 20 October 2015 – Accepted: 29 November 2015 – Published: 18 December 2015

Correspondence to: C.-H. Chan (hantijun@googlemail.com)

Published by Copernicus Publications on behalf of the European Geosciences Union.

NHESD

3, 7527–7553, 2015

**3-D grids and
time-dependent
factors for
earthquake
forecasting models**

C.-H. Chan

[Title Page](#)

[Abstract](#)

[Introduction](#)

[Conclusions](#)

[References](#)

[Tables](#)

[Figures](#)

[⏪](#)

[⏩](#)

[◀](#)

[▶](#)

[Back](#)

[Close](#)

[Full Screen / Esc](#)

[Printer-friendly Version](#)

[Interactive Discussion](#)



Abstract

This study provides some new insights into earthquake forecasting models to the regions with subduction systems, including the depth-component for forecasting grids and time-dependent factors. To manifest the importance of depth-component, I incorporate three-dimensional grids into forecasting approaches and compare with those with two-dimensional cells. Through applications to the two subduction regions, Ryukyu and Kanto, the approaches with three-dimensional grids always obtain better forecasting ability. I thus confirm the importance of depth-dependency for forecasting, especially for the applications to a subduction environment or a region with non-vertical seismogenic structures. In addition, I discuss the role of time-dependent factors for forecasting models. I conclude that time-dependency becomes crucial only when significant seismicity rate change follows a large earthquake. The insights into the applications of forecasting models could provide key information regarding seismic and tsunami hazard assessments.

1 Introduction

Earthquake forecasting models generally provide essential knowledge for seismic hazards mitigation, i.e. they point out the regions with high seismicity activity and provide fundamental information regarding seismic hazard assessment (Marzocchi et al., 2003; Lombardi and Marzocchi, 2009). Therefore, studies and interest in this issue have significantly increased and many forecasting models have been proposed.

However, most of the forecasting studies focus on the crustal earthquakes, i.e. their credibility remains controversial for the application to subduction environments. Such regions include non-vertical seismogenic structures, depth-independent grid cells thus become crucial for forecasting models. Besides of spatial distribution, temporal evolution of seismicity is another factor that dominates forecasting precision. Wiens et al. (1997) concluded that in comparison to crustal earthquakes sequence, a smaller

3-D grids and time-dependent factors for earthquake forecasting models

C.-H. Chan

[Title Page](#)

[Abstract](#)

[Introduction](#)

[Conclusions](#)

[References](#)

[Tables](#)

[Figures](#)

[⏪](#)

[⏩](#)

[◀](#)

[▶](#)

[Back](#)

[Close](#)

[Full Screen / Esc](#)

[Printer-friendly Version](#)

[Interactive Discussion](#)



number of aftershocks follows occurrence of a subduction event. Such differences in temporal behavior might result in forecasting bias.

Thus, this study applies several forecasting models and discusses their feasibility for the applications to subduction regions. To precisely model the behaviours of non-vertical seismogenic structures, I first develop approaches with three-dimensional grids cell. By comparing with those with two-dimensional cells, I manifest the importance of depth-component. To reveal the role of temporal factor for forecasting, I evaluate the forecasting ability of time-independent and renewal models. I apply the models to two subduction regions, the southwestern portion of the Ryukyu and Kanto.

2 Forecasting models

To examine the factors that control the feasibility of forecasting models in a subduction environment, this study introduces two forecasting approaches, the smoothing Kernel function and the rate-and-state friction model, described below.

2.1 The smoothing kernel function

Woo (1996) proposed a forecasting model, which described time-independent seismicity rate $\lambda(M, x)$ at the site of interest, x , as a function of magnitude, M , as follows:

$$\lambda(M, x) = \sum_{i=1}^{N_M} \frac{K(M, \overline{x - x_i})}{T_M}, \quad (1)$$

where $K(M, \overline{x - x_i})$ represents a smoothing Kernel as a function of magnitude and distance between the site of interest, x , and the location of the i th earthquake, x_i ; T_M represents the period of a complete catalog with a magnitude threshold; and N_M represents the total number of earthquakes with magnitudes larger than the threshold. This study follows the procedure of Woo (1996) and describe the Kernel function

3-D grids and time-dependent factors for earthquake forecasting models

C.-H. Chan

[Title Page](#)

[Abstract](#)

[Introduction](#)

[Conclusions](#)

[References](#)

[Tables](#)

[Figures](#)

[⏪](#)

[⏩](#)

[◀](#)

[▶](#)

[Back](#)

[Close](#)

[Full Screen / Esc](#)

[Printer-friendly Version](#)

[Interactive Discussion](#)



assumed plane. The law suggests that a positive ΔCFS enhances the occurrence of subsequent events, while a negative stress change inhibits future seismic activity. According to the law, however, Coulomb stress change model does not quantify seismicity rate changes.

To quantify seismicity rate evolution, Dieterich (1994) proposed the rate-and-state friction model. This model presents the evolution of the seismicity rate $\Delta R(M, x, t)$ by considering the n th source event $\Delta\text{CFS}_n(x)$ at the site of interest x as a function of magnitude, M , and time, t , as below:

$$\Delta R(M, x, t) = \frac{\lambda(M, x)}{\left[\frac{\lambda(M, x)}{\Delta R_{n-1}(M, x)} \exp\left(-\frac{\Delta\text{CFS}_n(x)}{A\sigma}\right) - 1 \right] \exp\left(-\frac{t-t_n}{t_{na}}\right) + 1}, \quad (5)$$

where $\lambda(M, x)$ represents the time-independent seismicity rate shown in Eq. (1); $\Delta R_{n-1}(M, x)$ represents the seismicity rate change just before the occurrence of the n th source event (i.e., $\Delta R_0 = \lambda(M, x)$); $A\sigma$ represents a constitutive parameter of the model with the dimension of a stress; t_n represents the occurrence time of the n th source event; and t_{na} represents the aftershock duration. The rate-and-state friction model forecasts the temporal evolution of seismicity rate after occurrence of large earthquakes.

3 Forecasting application to the Ryukyu region

3.1 Tectonic setting and earthquake catalog

The southwestern portion of the Ryukyu trench near Taiwan is seismically active since the Philippine Sea Plate subducts from the south to the Eurasian Plate (Fig. 1). In addition to high seismic activity, this region also contains an earthquake catalog with good quality. The Taiwan Telemetered Seismic Network (TTSN), the modern seismic network, initiated in the early 1970s (Tsai et al., 1981). Since the beginning of its operation, approximately 4000 earthquake events have been recorded each year. After

3-D grids and time-dependent factors for earthquake forecasting models

C.-H. Chan

[Title Page](#)

[Abstract](#)

[Introduction](#)

[Conclusions](#)

[References](#)

[Tables](#)

[Figures](#)

[I◀](#)

[▶I](#)

[◀](#)

[▶](#)

[Back](#)

[Close](#)

[Full Screen / Esc](#)

[Printer-friendly Version](#)

[Interactive Discussion](#)



the early 1990's, TTSN stations were integrated into the Central Weather Bureau Seismic Network (CWBSN), which records approximately 20 000 events each year (Shin, 1992). With a large amount of seismic activity and high quality earthquake catalogs, the region is an ideal site for earthquake forecasting test.

3.2 Procedure of application

3.2.1 The smoothing Kernel function

Implementing the earthquake catalog for a complete portion is a key factor for precise forecast. I checked magnitude of completeness, M_c , for the catalogs by the maximum curvature approach (Wiemer and Wyss, 2000). Due to station coverage, both of the TTSN and CWBSN catalogs (represented in Fig. 1a and b, respectively) obtain better observation quality inland than in the offshore region. The M_c for the CWBSN catalog (Fig. 1b) was lower than that for the TTSN (Fig. 1a) and the regions with a $M_c \leq 4.0$ for the TTSN and a $M_c \leq 3.0$ for the CWBSN are nearly the same. Thus, the intersection of the two catalogs, regions with $M_c \leq 4.0$ for TTSN and $M_c \leq 3.0$ for the CWBSN (Fig. 1c), determines our study region and the magnitude thresholds. I implemented the earthquakes before 2009 for model construction and referred those in 2010 and 2011 as forecasting events for retrospective test. Based on the earthquakes before 2009, the linear regression determined that the c and d values of the bandwidth function in Eq. (3) were 0.0174 km and 1.1209, respectively.

3.2.2 The rate-and-state friction model

To calculate ΔCFS , rupture behaviors of source earthquakes and mechanisms of receiver fault planes are two important factors. For the source earthquake parameters, I obtained the hypocenter location, the moment magnitude, and the focal mechanisms, through the Broadband Array in Taiwan for Seismology (BATS) website (<http://bats.earth.sinica.edu.tw/>) and determined fault dimension and magnitude of slip

3-D grids and time-dependent factors for earthquake forecasting models

C.-H. Chan

[Title Page](#)

[Abstract](#)

[Introduction](#)

[Conclusions](#)

[References](#)

[Tables](#)

[Figures](#)

[|◀](#)

[▶|](#)

[◀](#)

[▶](#)

[Back](#)

[Close](#)

[Full Screen / Esc](#)

[Printer-friendly Version](#)

[Interactive Discussion](#)



3-D grids and time-dependent factors for earthquake forecasting models

C.-H. Chan

[Title Page](#)

[Abstract](#)

[Introduction](#)

[Conclusions](#)

[References](#)

[Tables](#)

[Figures](#)

[⏪](#)

[⏩](#)

[◀](#)

[▶](#)

[Back](#)

[Close](#)

[Full Screen / Esc](#)

[Printer-friendly Version](#)

[Interactive Discussion](#)



through the scaling laws of Yen and Ma (2011). For receiver fault mechanisms, I followed the procedure of Catalli and Chan (2012) and assumed a spatially variable receiver fault plane for each calculation grid. A receiver fault plane for each grid consists with the closest reference focal mechanism determined by Wu et al. (2010). For each grid node, I evaluated the ΔCFS on both nodal planes and reported the higher value. To minimize depth uncertainty, this study followed the procedure of Catalli and Chan (2012) that evaluated the ΔCFS among seismogenic depth and reported the maximum value for each calculation grid. Since earthquakes with small magnitudes or those that have occurred far in the past do not significantly influence the current seismicity rate within the model (Catalli et al., 2008), I only analyzed the ΔCFS for the $M \geq 4.5$ events (Table 1). An intermediate value of $\mu' = 0.4$ was assumed for evaluating the ΔCFS . Application of the rate-and-state friction model requires parameters of $A\sigma$ and t_a . Previous studies (e.g. Toda and Stein, 2003; Toda et al., 2005; Catalli et al., 2008) have suggested that the physically reasonable range for $A\sigma$ is between 0.1 and 0.4 bars. I assumed a fixed $A\sigma$ of 0.2 bars, corresponding to the assumption of previous studies (e.g. Chan et al., 2012, 2013). t_a was assumed to be a function of the moment magnitude (M_w), as proposed by Burkhard and Grünthal (2009), described as follows:

$$t_a = e^{(-4.77 + \sqrt{0.62 + 17.32 \cdot M_w})} \text{ for } M_w < 7.8; \quad (6)$$

$$t_a = e^{(6.44 + 0.06 \cdot M_w)} \text{ for } M_w \geq 7.8. \quad (7)$$

The unit of t_a is in day. t_a is determined based on the magnitude of each source events (Table 1). I calculated the ΔCFS within a homogeneous half-space by applying the program of COULOMB 3.3 (Toda and Stein, 2002).

3.3 Results

3.3.1 The two-dimensional models

I first represent the forecasting models based on two-dimensional calculation cells with a $0.1^\circ \times 0.1^\circ$ size (i.e. the depth-independent model). For application of the smoothing

Kernel function, $x - x_j$ in Eq. (1) was the epicenter distance between the site of interest and the epicenter of earthquakes (i.e. depth-independent). The model forecasted higher rates along the coastline of Taiwan and for the area east of latitude 122.5° , which correspond to the distribution of the forecasting events during 2010 and 2011 (Fig. 2a).

For the Δ CFFS calculation on the two-dimensional grids, the target depth corresponds to the hypocentral depth of each source event (Table 1). Through the rate-and state friction model, I calculated the time-dependent rate evolutions for different moments (Fig. 3). In comparison with the spatio-temporal pattern of the forecasting events (open circles in Fig. 3), many of the consequent earthquakes are in the region with rate decrease (green stars in Fig. 3), i.e. the feasibility of this model is difficult to confirm.

3.3.2 The three-dimensional models

I then propose the forecasting models based on three-dimensional cells with $0.1^\circ \times 0.1^\circ \times 10$ km sizes (i.e. the depth-dependent model). For the smoothing Kernel function application, $x - x_j$ in Eq. (1) was the hypocenter distance between the site of interest and the hypocenter of earthquakes (i.e. depth-dependent). Two profiles along the longitudes of 122.0 and 122.5° (Fig. 2b and c, respectively) presented higher forecasted rates above the depth of 30 km and along the subduction slab dipping to the north, which fit the distribution of the forecasting earthquakes (the open circles in Fig. 2b and c) well.

For the rate-and-state friction model application, I evaluated the maximum Δ CFFS along the seismogenic depth for each cell and modeled the corresponding seismicity rate evolution (Fig. 4). Departing from the outcomes of the two-dimensional model (Fig. 3), a significant rate increase near the epicenter of each source event corresponds to the distribution of forecasting events (Fig. 4).

3-D grids and time-dependent factors for earthquake forecasting models

C.-H. Chan

[Title Page](#)

[Abstract](#)

[Introduction](#)

[Conclusions](#)

[References](#)

[Tables](#)

[Figures](#)

[⏪](#)

[⏩](#)

[◀](#)

[▶](#)

[Back](#)

[Close](#)

[Full Screen / Esc](#)

[Printer-friendly Version](#)

[Interactive Discussion](#)



4 Forecasting application to the Kanto region

4.1 Tectonic setting and earthquake catalog

The Kanto, Japan, region is an area with complex tectonic setting. Most parts of this region sit on the Eurasian Plate, under which the Philippine Sea Plate subducts from the south. At further depth, the Pacific Plate subducts from the east (Toda et al., 2008). The complex plate interactions in this region result in seismic activity. Fortunately, this region has not only high seismic activity but also a high-quality earthquake catalog. The modern seismic network maintained by the Japan Meteorological Agency (JMA) Network was initiated in 1923 and has been modernized over time (Nanjo et al., 2010). In addition, significant change in the seismicity behavior in the Kanto region followed the 2011 $M9.0$ Tohoku earthquake (Ishibe et al., 2011; Toda et al., 2011). Such spatial-temporal condition provides an ideal environment for testing credibility of forecasting models in respect of both depth and time factors.

4.2 Procedure of application

Due to the seismic network modernization, M_c of the JMA catalog decreased dramatically after 1980 and 1990, respectively (Nanjo et al., 2010). Thus, I analyzed the catalog with various magnitude threshold in the three periods: magnitudes 4.5, 3.5 and 2.5 for 1923–1979, 1980–1989 and 1990–2011, respectively. The thresholds correspond to the M_c determined by Nanjo et al. (2010) through the Entire Magnitude Range (EMR) method (Woessner and Wiemer, 2005). I input the complete part of the JMA catalog until the end of 2009 for forecast model construction, and referred those in 2010 and 2011 for retrospective test. The linear regression determined that the c and d values of the bandwidth function were 0.9271 km and 0.6722, respectively. The parameters obtained above provide basis for application of the smoothing Kernel approach.

For the forecast using the rate-and-state friction model, I calculated the ΔCFS for the $M \geq 6.0$ events during 2010 and 2011 (Fig. 5). The ΔCFS calculation for the 2011

3-D grids and time-dependent factors for earthquake forecasting models

C.-H. Chan

[Title Page](#)

[Abstract](#)

[Introduction](#)

[Conclusions](#)

[References](#)

[Tables](#)

[Figures](#)

[⏪](#)

[⏩](#)

[◀](#)

[▶](#)

[Back](#)

[Close](#)

[Full Screen / Esc](#)

[Printer-friendly Version](#)

[Interactive Discussion](#)



3-D grids and time-dependent factors for earthquake forecasting models

C.-H. Chan

[Title Page](#)

[Abstract](#)

[Introduction](#)

[Conclusions](#)

[References](#)

[Tables](#)

[Figures](#)

[⏪](#)

[⏩](#)

[◀](#)

[▶](#)

[Back](#)

[Close](#)

[Full Screen / Esc](#)

[Printer-friendly Version](#)

[Interactive Discussion](#)

M9.0 Tohoku earthquake is based on the coseismic dislocation model obtained by tsunami waveform inversion (Fujii et al., 2011). For the rest of the source events, I obtained the parameters by the F-net catalog maintained by National Research Institute for Earth Science and Disaster Prevention, Japan (NIED) (<http://www.fnet.bosai.go.jp/event/search.php?LANG=en>) and determined fault dimension and magnitude of slip through the scaling laws proposed by Wells and Coppersmith (1994). A receiver fault plane for each grid consists with the closest reference focal mechanism from the F-net catalog.

4.3 Results

4.3.1 The two-dimensional model

This study first forecasts on two-dimensional calculation cells with $0.2^\circ \times 0.2^\circ$ sizes defined by the Collaboratory for the Study of Earthquake Predictability (CSEP) Japan Testing Center for the Kanto region (Tsuruoka et al., 2012). The target depth for the Δ CFS calculation is 47.5 km, which corresponds to the averaged hypocentral depth of the earthquakes in the region. The models represent higher seismicity rates for smaller magnitude ranges (e.g. Fig. 6a) than for larger ones (e.g. Fig. 6d), consisting with the Gutenberg–Richter law (Gutenberg and Richter, 1954). In addition, due to stress-enhanced by the Tohoku sequence (Ishibe et al., 2011; Todal et al., 2011), high seismicity rate is forecasted along the coast and at the offshore of the Pacific Ocean and 40 km northeast of Tokyo. Note that the stress shadow zone at the target depth by the source events (including the 2011 Tohoku mainshock) resulted in some low forecasted-rate zones at offshore of the Pacific Ocean.

4.3.2 The three-dimensional model

I then proposed a depth-dependent model based on three-dimensional cells with $0.2^\circ \times 0.2^\circ \times 5$ km sizes. Comparing with the forecast with two-dimensional cells, the

three-dimensional model illustrated detailed patterns along the depth (Fig. 7b–d), e.g. the high seismicity rate at 40 km northeast of Tokyo is identified at depths in between 30 and 70 km (Fig. 7b); the high rate along the coast and at the offshore of the Pacific Ocean locates at the depth of 25–75 km (Fig. 7d), consistent with the boundary between the Pacific and Eurasia Plates (Toda et al., 2008).

5 Discussion and conclusion

5.1 Importance of the temporal factor

Since the smoothing Kernel function averages the seismic activity during the observation period, it can be regarded as a time-independent model. On the contrary, the rate-and-state friction model forecasts temporal evolution of seismicity rate disturbed by a series of source events and can be renewed with time. The comparison between the two models may indicate the importance of the temporal factor for forecasting.

To validate the forecasting ability statistically, I compared models with the distribution of forecasting earthquakes through the Molchan diagram (Molchan, 1990). In the diagram, the “fraction of alarm-occupied space” indicates the percentage of events within the study region with a forecasting level equal to or higher than “alarm”. The “fraction of failure in forecasting” represents the percentage of consequent earthquakes having a lower forecasting level than the alarm. In the diagram, when data points distribute along a diagonal line, the distribution of target earthquakes is independent of forecasting; convex distribution suggests that the majority of consequent earthquakes occur within regions with a lower forecasted rate, whereas concavity suggests that the majority of consequent earthquakes are within high forecasted rate area.

In the Ryukyu case, only 28% of the forecasted earthquakes were located in the area with a low (≤ 50 percentile) forecasted rate by the smoothing Kernel model using the two-dimensional grids (the blue dots in Fig. 8). On the other hand, the rate-and-state friction model (the red dots in Fig. 8) forecasted 39% of the earthquakes for the

3-D grids and time-dependent factors for earthquake forecasting models

C.-H. Chan

[Title Page](#)

[Abstract](#)

[Introduction](#)

[Conclusions](#)

[References](#)

[Tables](#)

[Figures](#)

[⏪](#)

[⏩](#)

[◀](#)

[▶](#)

[Back](#)

[Close](#)

[Full Screen / Esc](#)

[Printer-friendly Version](#)

[Interactive Discussion](#)



3-D grids and time-dependent factors for earthquake forecasting models

C.-H. Chan

[Title Page](#)

[Abstract](#)

[Introduction](#)

[Conclusions](#)

[References](#)

[Tables](#)

[Figures](#)

[⏪](#)

[⏩](#)

[◀](#)

[▶](#)

[Back](#)

[Close](#)

[Full Screen / Esc](#)

[Printer-friendly Version](#)

[Interactive Discussion](#)



same condition, suggesting less forecasting ability. I obtain similar conclusion for the three-dimensional model. The smoothing Kernel function (the yellow dots in Fig. 8) and rate-and-state friction model (the green dots in Fig. 8) forecast 13 and 36 % forecasted earthquakes located within the area with low rates. Therefore, regardless the dimension of calculation grids, the smoothing Kernel model provides a better forecasting ability. This finding corresponds to the conclusion of Chan et al. (2012), obtained from forecasting experience in entire Taiwan. For the Kanto case, the rate-and-state friction model forecast only 5 % of events that are located within the low forecast rate area, that is significant fewer in comparing with 23 %, forecasted by the Kernel model (Fig. 9). Thus, departing from conclusion of the Ryukyu case, the rate-and-state friction model provides a better performance.

The discrepant conclusions between the two cases might be attributed to the effect of recent earthquakes. For the cases of Ryukyu and Chan et al. (2012), there was no significant short-term rate perturbation during the forecasting periods. For the Kanto case, on the contrary, the time-dependency becomes a crucial factor to forecast the consequence after the 2011 Tohoku earthquake (Ishibe et al., 2011; Toda et al., 2011).

5.2 Importance of the depth factor

Both of the Ryukyu and Kanto cases have qualitatively shown that three-dimensional models have a better performance in Figs. 2 and 7, respectively. The smoothing Kernel function using three-dimensional grids forecasted distribution along depth in detail. For the rate-and-state friction model, the three-dimensional applications presented significant rate increase for most regions near the epicenter of each source event, corresponds to the distribution of forecasting events.

For the Ryukyu application, comparing between forecasted rates obtained using the smoothing Kernel function and the locations of target earthquakes using the Molchan diagram (Fig. 8), the three-dimensional forecasting model had a better forecasting ability, i.e. a smaller fraction of failure to predict. In addition, the ratio of the forecasting earthquakes located within the area having a low forecast rate using two- and

3-D grids and time-dependent factors for earthquake forecasting models

C.-H. Chan

[Title Page](#)

[Abstract](#)

[Introduction](#)

[Conclusions](#)

[References](#)

[Tables](#)

[Figures](#)

[⏪](#)

[⏩](#)

[◀](#)

[▶](#)

[Back](#)

[Close](#)

[Full Screen / Esc](#)

[Printer-friendly Version](#)

[Interactive Discussion](#)

three-dimensional models are 28 % and 13, respectively. For the rate-and-state friction model, the three-dimensional applications grids also provide a better forecasting ability (green dots in Fig. 8) in comparison to the two-dimensional one (red dots in Fig. 8).

The application to the Kanto region also confirmed the better performance of the three-dimensional models. In the three-dimensional model, only 3 % of forecasting earthquakes were located within the study area having a high forecast rate change (green dots in Fig. 9). It is significantly higher than 64 % of that reported by the two-dimensional model (yellow dots in Fig. 9). In addition, in the Kanto case, the Molchan diagram raised the disadvantage for the rate-and-state model using two dimensional calculation grids. When the fraction of alarm-occupied space is large, convex distributions are presented (red and yellow dots in Fig. 9), i.e. some earthquakes took place in the region with low/no forecasted rates (region in white in Fig. 6), suggesting forecasting failure. In contrast with the two-dimensional models, the three-dimensional ones have proved their forecasting ability (green dots in Fig. 9). The conclusion is consistent with the findings of Catalli and Chan (2012) and confirm that the depth-factor is one of the most important parameters for Coulomb stress calculation.

Through the applications to different forecasting approaches, I have confirmed that models with three-dimensional grids always obtain better forecasting ability. I thus determined the importance of depth-dependency for forecasting models, especially for the application to a subduction environment or within a region with non-vertical seismic structures.

5.3 Application to seismic hazard assessments and corresponding hazard mitigation

A lot of subduction events, which resulted in severe damage and fatality due to ground shaking and tsunami, emphasized the importance of depth-dependent forecasting models. For example, an M_w 7.1 earthquake took place on 31 March 2002 in the southwestern portion of the Ryukyu subduction system. Although Taipei is more than 100 km away from the epicenter, ground shaking led to the toppling of two construction cranes

3-D grids and time-dependent factors for earthquake forecasting models

C.-H. Chan

[Title Page](#)

[Abstract](#)

[Introduction](#)

[Conclusions](#)

[References](#)

[Tables](#)

[Figures](#)

[⏪](#)

[⏩](#)

[◀](#)

[▶](#)

[Back](#)

[Close](#)

[Full Screen / Esc](#)

[Printer-friendly Version](#)

[Interactive Discussion](#)

constructing Taipei 101, the tallest building in Taiwan. This case indicated the potential seismic hazard from the intraslab earthquakes, which take place in the deeper part of the subduction zone. The seismic energy generated by these earthquakes does not decay significantly with travel distance, especially for the long-period response spectra (Lin and Lee, 2008). Such behavior could result in seismic hazards, especially for high-rise buildings. Another example of the hazard from megathrusts is the 2011 *M*9.0 Tohoku earthquake, which resulted in a devastating tsunami. Due to large displacements (up to 60 m) at shallow depth (Lay et al., 2011), significant seafloor deformation leads to the tsunami.

The two examples raise the importance of precise hypocentral depth for forecasting models in regards to consequent hazard mitigation for ground shaking and tsunami. This study has provided some insights into the applications of forecasting models and concluded the importance of depth factor. It could provide key information regarding seismic and tsunami hazard assessments.

Acknowledgements. Our work was supported by the Earthquake Research Institute, University of Tokyo. The author would like to thank CWB, JMA and NIED for providing the earthquake catalogs used in this study and Stefano Tinti for the constructive comments.

References

- Beuval, C., Scotti, O., and Bonilla, F.: The role of seismicity models in probabilistic seismic hazard estimation: comparison of a zoning and a smoothing approach, *Geophys. J. Int.*, 165, 584–595, 2006.
- Burkhard, M. and Grünthal, G.: Seismic source zone characterization for the seismic hazard assessment project PEGASOS by the Expert Group 2 (EG 1b), *Swiss J. Geosci.*, 102, 149–188, 2009.
- Catalli, F. and Chan, C. H.: New insights into the application of the Coulomb model in real-time, *Geophys. J. Int.*, 188, 583–599, doi:10.1111/j.1365-246X.2011.05276.x, 2012.

3-D grids and time-dependent factors for earthquake forecasting models

C.-H. Chan

[Title Page](#)[Abstract](#)[Introduction](#)[Conclusions](#)[References](#)[Tables](#)[Figures](#)[⏪](#)[⏩](#)[◀](#)[▶](#)[Back](#)[Close](#)[Full Screen / Esc](#)[Printer-friendly Version](#)[Interactive Discussion](#)

- Catalli, F., Cocco, M., Console, R., and Chiaraluca, L.: Modeling seismicity rate changes during the 1997 Umbria-Marche sequence (central Italy) through a rate- and state-dependent model, *J. Geophys. Res.*, 113, B11301, doi:10.1029/2007JB005356, 2008.
- Chan, C. H., Sørensen, M. B., Stromeyer, D., Grünthal, G., Heidbach, O., Hakimhashemi, A., and Catalli, F.: Forecasting Italian seismicity through a spatio-temporal physical model: importance of considering time dependency and reliability of the forecast, *Ann. Geophys.-Italy*, 53, 129–140, doi:10.4401/ag-4761, 2010.
- Chan, C.-H., Wu, Y.-M., and Wang, J.-P.: Earthquake forecasting using the rate-and-state friction model and a smoothing Kernel: application to Taiwan, *Nat. Hazards Earth Syst. Sci.*, 12, 3045–3057, doi:10.5194/nhess-12-3045-2012, 2012.
- Chan, C. H., Wu, Y. M., Cheng, C. T., Lin, P. S., and Wu, Y. C.: Time-dependent probabilistic seismic hazard assessment and its application to Hualien City, Taiwan, *Nat. Hazards Earth Syst. Sci.*, 13, 1–16, doi:10.5194/nhess-13-1-2013, 2013.
- Cocco, M., Rice, J. R.: Pore pressure and poroelasticity effects in Coulomb stress analysis of earthquake interactions, *J. Geophys. Res.*, 107, 2030, doi:10.1029/2000JB000138, 2002.
- Dieterich, J. H.: A constitutive law for rate of earthquake production and its application to earthquake clustering, *J. Geophys. Res.*, 99, 2601–2618, 1994.
- Fujii, Y., Satake, K., Sakai, S., Shinohara, M., and Kanazawa, T.: Tsunami source of the 2011 off the Pacific coast of Tohoku Earthquake, *Earth Planets Space*, 63, 815–820, 2011.
- Gutenberg, B. and Richter, C.: *Seismicity of the Earth and Associated Phenomena*, 2nd ed., Princeton University Press, Princeton, USA, 1954.
- Harris, R. A.: Introduction to special section, Stress triggers, stress shadows, and implications for seismic hazard, *J. Geophys. Res.*, 103, 24347–24358, 1998.
- Ishibe, T., Shimazaki, K., Satake, K., and Tsuruoka, H.: Change in seismicity beneath the Tokyo metropolitan area due to the 2011 off the Pacific coast of Tohoku earthquake, *Earth Planets Space*, 63, 731–735, doi:10.5047/eps.2011.06.001, 2011.
- Lay, T., Ammon, C. J., Kanamori, H., Xue, L., and Kim, M. J.: Possible large near-trench slip during the 2011 $M(w)9.0$ off the Pacific coast of Tohoku Earthquake, *Earth Planets Space*, 63, 687–692, 2011.
- Lin, P. S. and Lee, C. T.: Ground-motion attenuation relationships for subduction-zone earthquakes in northeastern Taiwan, *B. Seismol. Soc. Am.*, 98, 220–240, doi:10.1785/0120060002, 2008.

3-D grids and time-dependent factors for earthquake forecasting models

C.-H. Chan

[Title Page](#)[Abstract](#)[Introduction](#)[Conclusions](#)[References](#)[Tables](#)[Figures](#)[⏪](#)[⏩](#)[◀](#)[▶](#)[Back](#)[Close](#)[Full Screen / Esc](#)[Printer-friendly Version](#)[Interactive Discussion](#)

- Lombardi, A. M. and Marzocchi, W.: Double Branching model to forecast the next $M \geq 5.5$ earthquakes in Italy, *Tectonophysics*, 475, 514–523, 2009.
- Marzocchi, W., Sandri, L., and Boschi, E.: On the validation of earthquake-forecasting models: the case of pattern recognition algorithms, *B. Seismol. Soc. Am.*, 93, 1994–2004, 2003.
- 5 Molchan, G. M.: Strategies in strong earthquake prediction, *Phys. Earth Planet. In.*, 61, 84–98, 1990.
- Molina, S., Lindholm, C. D., and Bungum, H., Probabilistic seismic hazard analysis: zoning free versus zoning methodology, *B. Geofis. Teor. Appl.*, 42, 19–39, 2001.
- Nanjo, K. Z., Ishibe, T., Tsuruoka, H., Schorlemmer, D., Ishigaki, Y., and Hirata, N.: Analysis
10 of the completeness magnitude and seismic net-work coverage of Japan, *B. Seismol. Soc. Am.*, 100, 3261–3268, doi:10.1785/0120100077, 2010.
- Shin, T. C.: Some implications of Taiwan tectonic features from the data collected by the Central Weather Bureau Seismic Network, *Meteorology Bulletin*, 38, 23–48, 1992 (in Chinese).
- Tsuruoka, H., Hirata, N., Schorlemmer, D., Euchner, F., Nanjo, K. Z., and Jordan, T. H.: CSEP
15 Testing Center and the first results of the earthquake forecast testing experiment in Japan, *Earth Planets Space*, 64, 661–671, 2012.
- Toda, S. and Stein, R. S.: Toggling of seismicity by the 1997 Kagoshima earthquake couplet: a demonstration of time-dependent stress transfer, *J. Geophys. Res.*, 108, 2567, doi:10.1029/2003JB002527, 2003.
- 20 Toda, S., Stein, R. S., Richards-Dinger, K., and Bozkurt, S. B.: Forecasting the evolution of seismicity in southern California: Animations built on earthquake stress transfer, *J. Geophys. Res.*, 110, B05S16, 2005.
- Toda, S., Stein, R. S., Kirby, S. H., and Bozkurt, S. B.: A slab fragment wedged under Tokyo and its tectonic and seismic implications, *Nat. Geosci.*, 1, 1–6, doi:10.1038/ngeo1318, 2008.
- 25 Toda, S., Stein, R. S., and Lin, J.: Widespread seismicity excitation throughout central Japan following the 2011 $M = 9.0$ Tohoku earthquake and its interpretation by Coulomb stress transfer, *Geophys. Res. Lett.*, 38, L00G03, doi:10.1029/2011GL047834, 2011.
- Tsai, Y. B., Liaw, Z. S., and Lee, T. Q.: A statistical study of the Taiwan Telemetered Seismographic Network data during 1973–1979, *Bulletin Institute of Earth Sciences, Academia Sinica*, 1, 1–22, 1981.
- 30 Wells, D. L. and Coppersmith, K. J.: New empirical relationships among magnitude, rupture length, rupture width, rupture area, and surface displacement, *B. Seismol. Soc. Am.*, 84, 974–1002, 1994.

3-D grids and time-dependent factors for earthquake forecasting models

C.-H. Chan

[Title Page](#)[Abstract](#)[Introduction](#)[Conclusions](#)[References](#)[Tables](#)[Figures](#)[|◀](#)[▶|](#)[◀](#)[▶](#)[Back](#)[Close](#)[Full Screen / Esc](#)[Printer-friendly Version](#)[Interactive Discussion](#)

Wiemer, S. and Wyss, M.: Minimum Magnitude of Completeness in Earthquake Catalogs: examples from Alaska, the Western United States, and Japan, *B. Seismol. Soc. Am.*, 90, 859–869, 2000.

5 Wiens, D. A., Gilbert, H. J., Hicks, B., Wyssession, M. E., and Shore, P. J.: Aftershock sequences of moderate-sized intermediate and deep earthquakes in the Tonga Subduction Zone, *Geophys. Res. Lett.*, 24, 2059–2062, 1997.

Woessner, J. and Wiemer, S.: Assessing the quality of earthquake catalogues: estimating the magnitude of completeness and its uncertainty, *B. Seismol. Soc. Am.*, 95, 684–698, doi:10.1785/0120040007, 2005.

10 Woo, G.: Kernel estimation methods for seismic hazard area source modeling, *B. Seismol. Soc. Am.*, 86, 353–362, 1996.

Wu, Y. M., Hsu, Y. J., Chang, C. H., Teng, L. S., and Nakamura, M.: Temporal and spatial variation of stress field in Taiwan from 1991 to 2007: insights from comprehensive first motion focal mechanism catalog, *Earth Planet. Sc. Lett.*, 298, 306–316, doi:10.1016/j.epsl.2010.07.047, 2010.

15 Yen, Y. T. and Ma, K. F.: Source-scaling relationship for $M_{4.6}$ –8.9 earthquakes, specifically for earthquakes in the collision zone of Taiwan, *B. Seismol. Soc. Am.*, 101, 464–481, doi:10.1785/0120100046, 2011.

3-D grids and time-dependent factors for earthquake forecasting models

C.-H. Chan

Table 1. Source parameters for the source events used for the inputs of the rate-and-state friction model. Earthquakes with $M_w \geq 4.5$ that occurred in 2010 and 2011 were considered. Parameters were determined based on the Broadband Array in Taiwan for Seismology (BATS).

| No. of event | Year | Month | Day | Longitude (° E) | Latitude (° N) | Depth (km) | M_w | Strike (°) | Dip (°) | Rake (°) |
|--------------|------|-------|-----|-----------------|----------------|------------|-------|------------|---------|----------|
| 1 | 2010 | 2 | 26 | 122.84 | 23.60 | 44 | 5.0 | 200.9 | 33.8 | 97.7 |
| 2 | 2010 | 6 | 15 | 121.63 | 24.06 | 16 | 5.1 | 261.3 | 42.8 | 142.5 |
| 3 | 2010 | 7 | 8 | 122.00 | 24.40 | 24 | 4.7 | 290.6 | 21.4 | -110.9 |
| 4 | 2010 | 7 | 9 | 122.66 | 24.66 | 116 | 4.8 | 216.5 | 60.9 | 20.4 |
| 5 | 2010 | 8 | 30 | 122.11 | 24.92 | 11 | 4.6 | 189.8 | 26.5 | -141.1 |
| 6 | 2010 | 11 | 12 | 122.43 | 24.05 | 29 | 4.6 | 327.7 | 65.9 | 160.4 |
| 7 | 2010 | 11 | 21 | 121.75 | 23.83 | 46 | 5.2 | 248.9 | 22.4 | 141.3 |
| 8 | 2011 | 2 | 1 | 121.80 | 24.24 | 23 | 4.9 | 329.1 | 27.7 | -131.0 |
| 9 | 2011 | 5 | 22 | 121.72 | 24.15 | 19 | 4.7 | 215.1 | 63.9 | -4.3 |

[Title Page](#)[Abstract](#)[Introduction](#)[Conclusions](#)[References](#)[Tables](#)[Figures](#)[⏪](#)[⏩](#)[◀](#)[▶](#)[Back](#)[Close](#)[Full Screen / Esc](#)[Printer-friendly Version](#)[Interactive Discussion](#)

3-D grids and time-dependent factors for earthquake forecasting models

C.-H. Chan

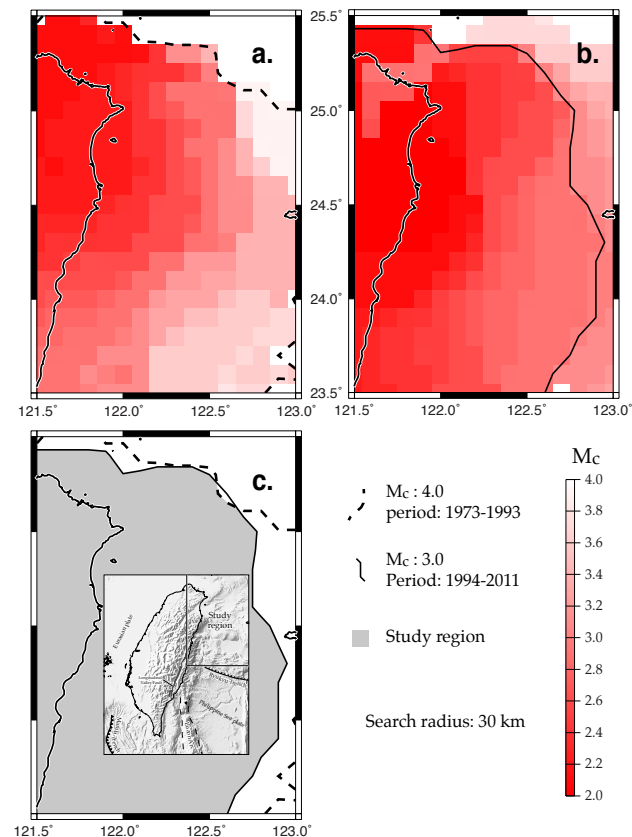


Figure 1. The magnitude of completeness (M_c) for (a) the TTSN and (b) the CWBSN catalogs. (c) The study area shown in gray, with the intersection of regions with $M_c \leq 4.0$ for the TTSN shown with dashed lines and with $M_c \leq 3.0$ for the CWBSN shown with solid lines. The M_c for each grid is determined according to the events that occurred within 30 km from center of each grid.

3-D grids and time-dependent factors for earthquake forecasting models

C.-H. Chan

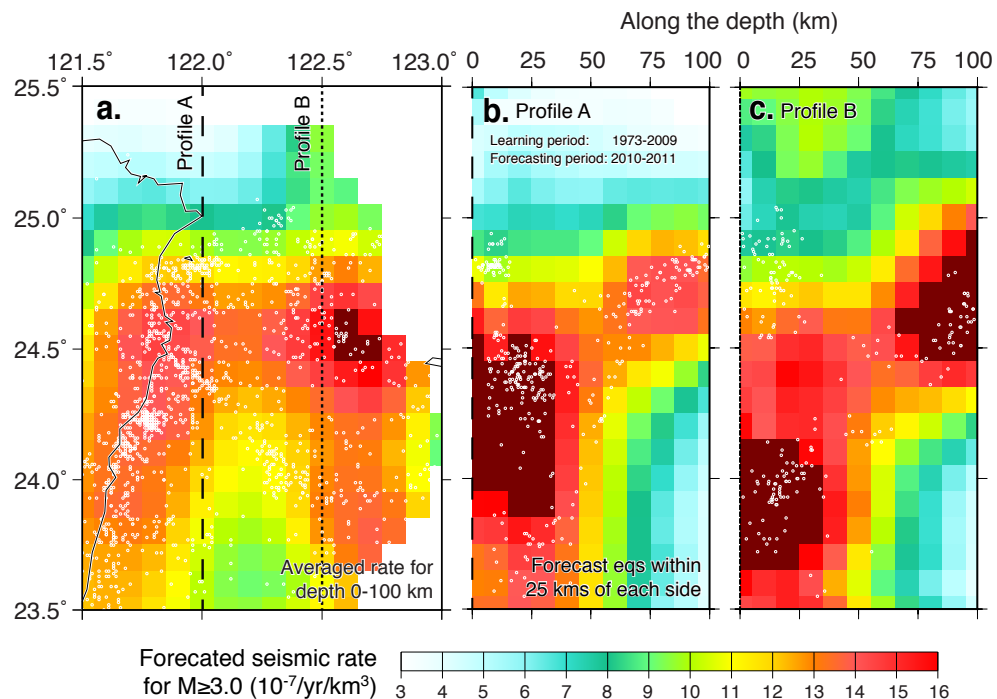


Figure 2. (a) A map-view and (b–c) profiles of the forecasted seismicity rate for $M \geq 3.0$ modeled by the epicenter-smoothing Kernel function. White circles denote the earthquakes from 2010 to 2011. Earthquakes within 25 km of each side of the profiles are presented.

[Title Page](#)
[Abstract](#)
[Introduction](#)
[Conclusions](#)
[References](#)
[Tables](#)
[Figures](#)
[⏪](#)
[⏩](#)
[◀](#)
[▶](#)
[Back](#)
[Close](#)
[Full Screen / Esc](#)
[Printer-friendly Version](#)
[Interactive Discussion](#)

3-D grids and time-dependent factors for earthquake forecasting models

C.-H. Chan

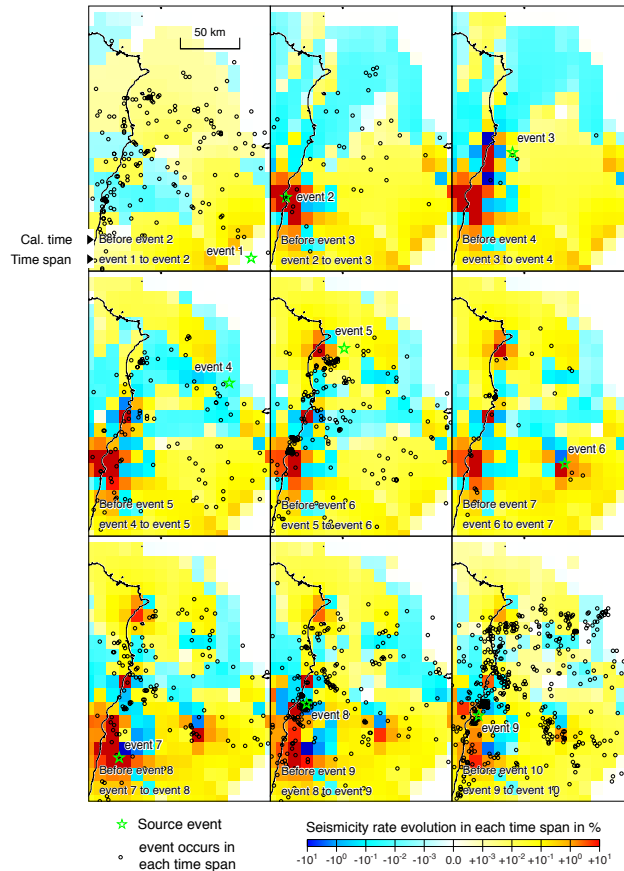


Figure 3. The seismicity rate evolution at different time moments. The target depth for the Δ CFS calculation corresponds to the hypocentral depth of each source event (Table 1). Source events from 2010 to 2011 are shown as open green stars. Open circles denote earthquakes during each time sequence.

[Title Page](#)

[Abstract](#)

[Introduction](#)

[Conclusions](#)

[References](#)

[Tables](#)

[Figures](#)

[⏪](#)

[⏩](#)

[⏴](#)

[⏵](#)

[Back](#)

[Close](#)

[Full Screen / Esc](#)

[Printer-friendly Version](#)

[Interactive Discussion](#)



3-D grids and time-dependent factors for earthquake forecasting models

C.-H. Chan

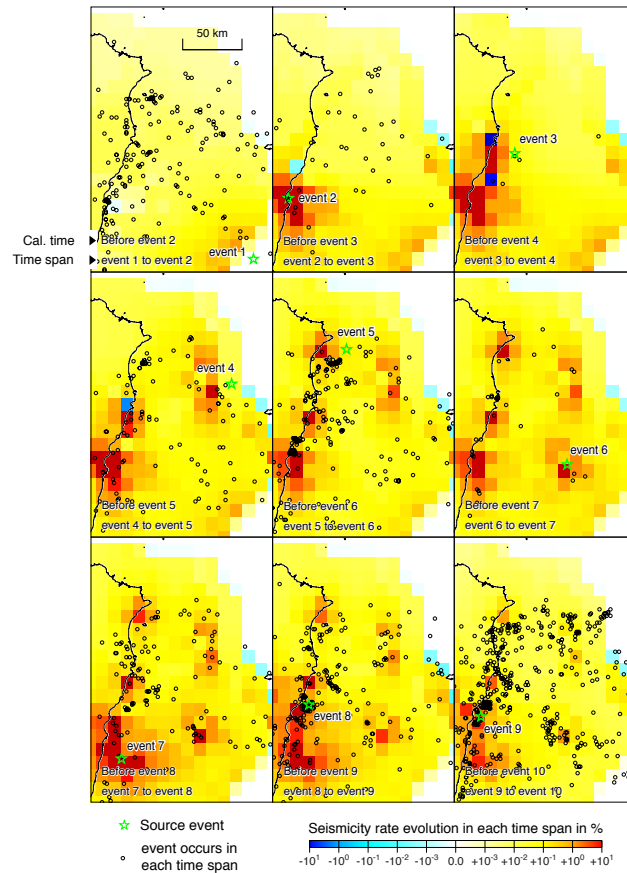


Figure 4. The seismicity rate evolution at different time moments. The Δ CFS for each grid is defined as the maximum Coulomb stress changes among the entire seismogenic depth. Source parameters for the source events for calculating are shown in Table 1.

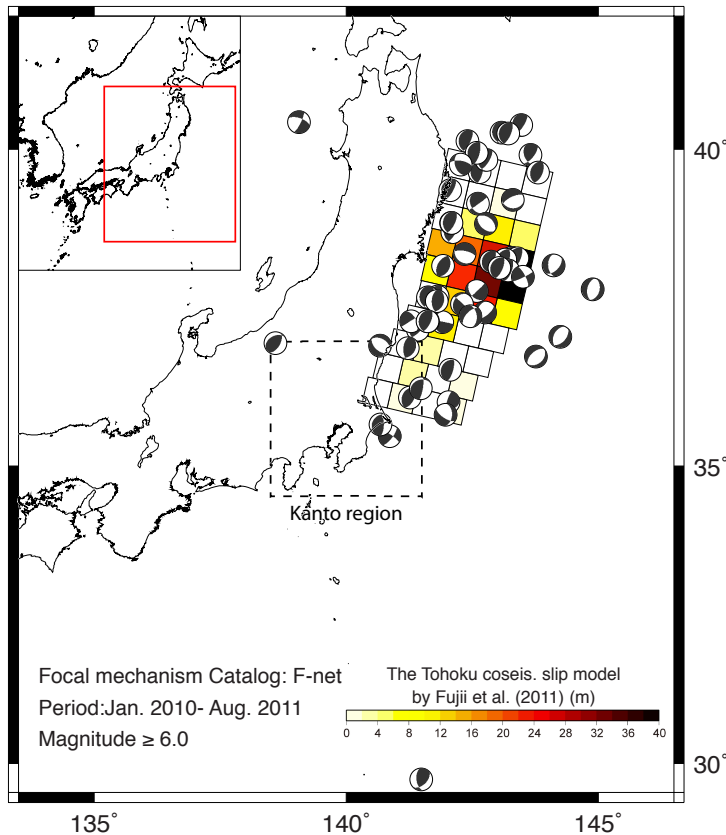


Figure 5. Distribution of the $M \geq 6.0$ earthquakes during January 2010 and August 2011, which took place in or near the Kanto region. The coseismic dislocation model of the 2011 $M9.0$ Tohoku earthquake is obtained by tsunami waveform inversion (Fujii et al., 2011), whereas the focal mechanisms of the others are obtained from the F-net catalog.

3-D grids and time-dependent factors for earthquake forecasting models

C.-H. Chan

[Title Page](#)

[Abstract](#)

[Introduction](#)

[Conclusions](#)

[References](#)

[Tables](#)

[Figures](#)

[⏪](#)

[⏩](#)

[◀](#)

[▶](#)

[Back](#)

[Close](#)

[Full Screen / Esc](#)

[Printer-friendly Version](#)

[Interactive Discussion](#)



3-D grids and time-dependent factors for earthquake forecasting models

C.-H. Chan

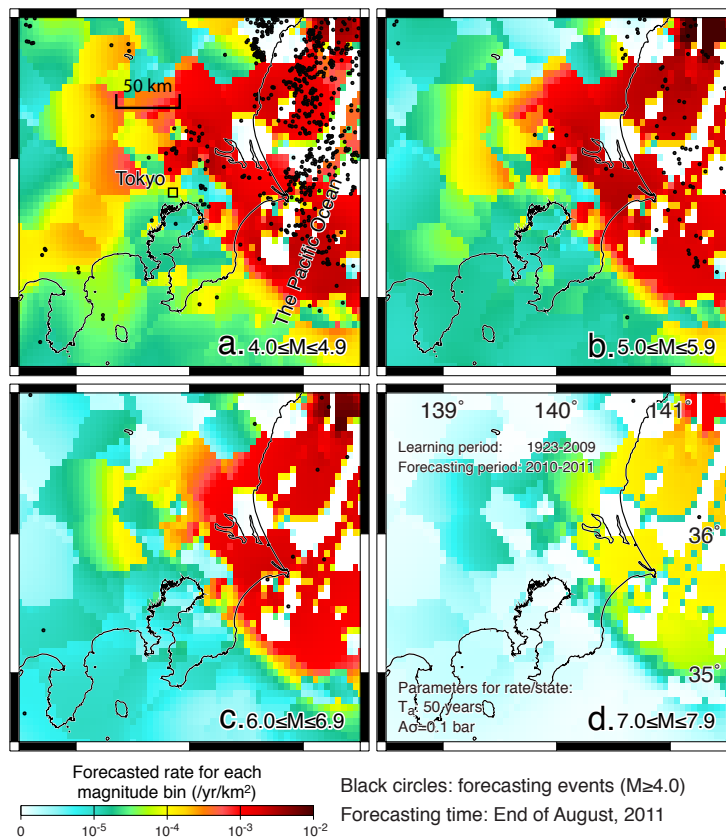


Figure 6. The two-dimensional forecasting models for the magnitudes in between (a) 4.0 and 4.9; (b) 5.0 and 5.9; (c) 6.0 and 6.9; and (d) 7.0 and 7.9, respectively, in the end of August 2011. Black dots denote the $M \geq 4.0$ earthquakes during January 2010 and August 2011.

3-D grids and time-dependent factors for earthquake forecasting models

C.-H. Chan

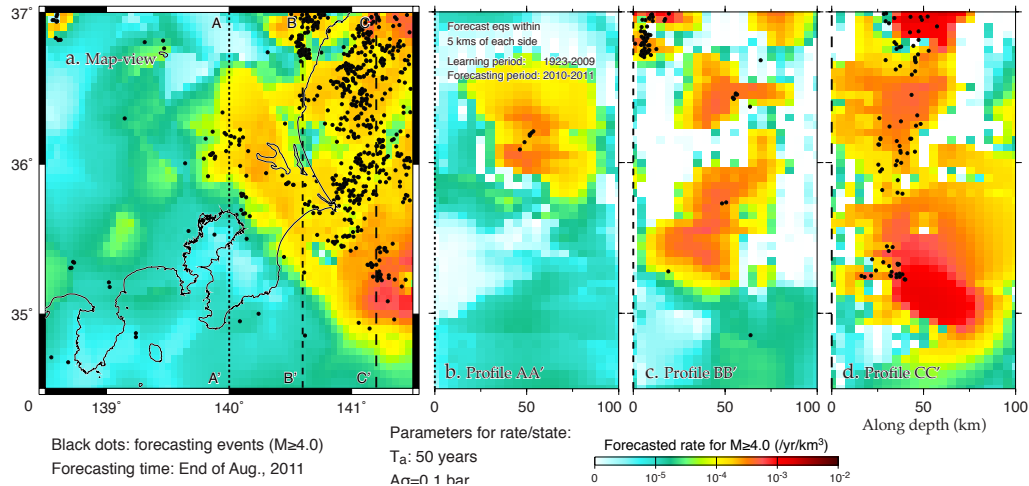


Figure 7. (a) Map-view, and (b–d) profiles of the three-dimensional forecasting models in the end of August 2011 and the distribution of the target earthquakes during 2010–2011. Black dots represent the earthquakes during 2010–2011. Black dots denote the $M \geq 4.0$ earthquakes during January 2010 and August 2011. Earthquakes within 5 km of each side of the profiles are presented.

3-D grids and time-dependent factors for earthquake forecasting models

C.-H. Chan

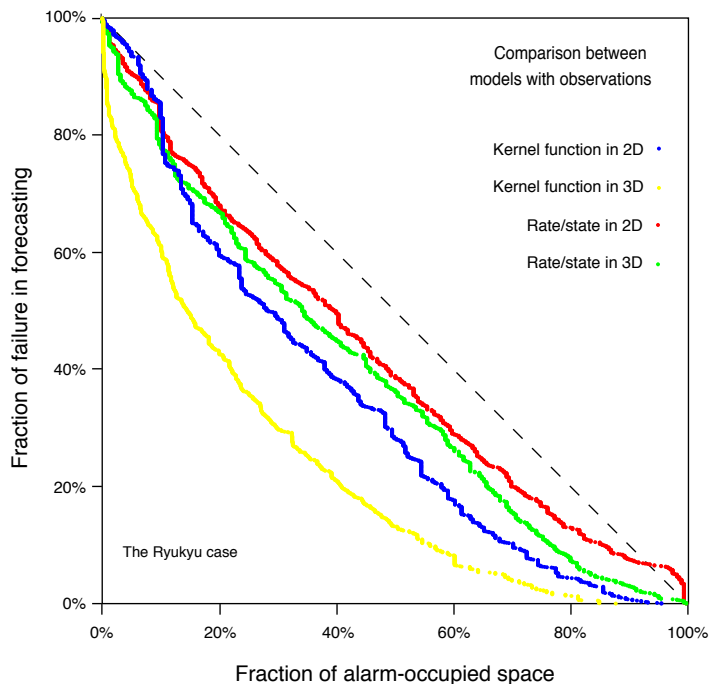


Figure 8. The Molchan diagram used for investigating the correlation between different forecasting models and earthquakes during the forecasting period (2010–2011) for the Ryukyu case. Blue and yellow dots represent the results for the models using the smoothing Kernel models in two- and three-dimensional grids, respectively; red and green dots represent the results for the models using the rate-and-state friction models in two- and three-dimensional grids, respectively.

3-D grids and time-dependent factors for earthquake forecasting models

C.-H. Chan

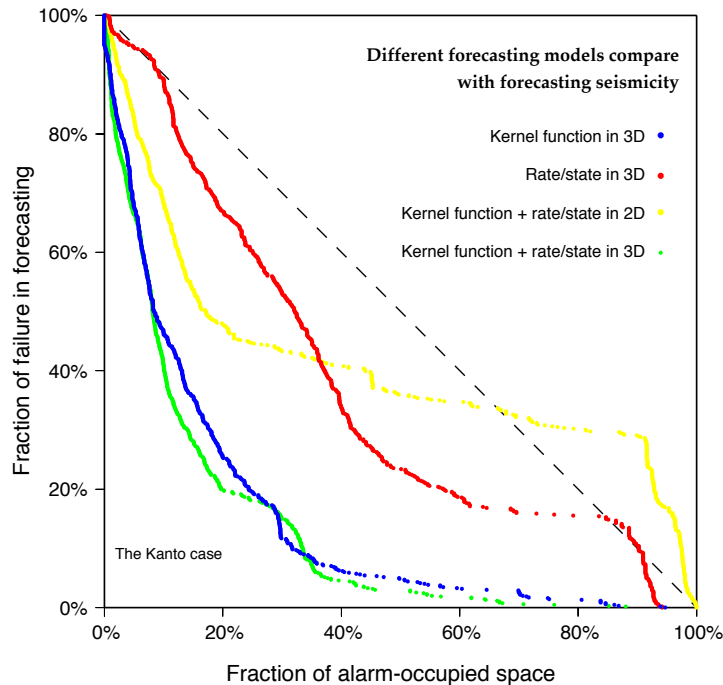


Figure 9. The Molchan diagram used for investigating the correlation between different forecasting models and earthquakes during the forecasting period (January 2010–August 2011) for the Kanto case. Blue and red dots denote the results for the models using the smoothing Kernel function and the rate-and-state friction model, respectively; yellow and green dots denote the results for the combination models in two- and three-dimensional grids, respectively.

[Title Page](#)

[Abstract](#)

[Introduction](#)

[Conclusions](#)

[References](#)

[Tables](#)

[Figures](#)

⏪

⏩

◀

▶

[Back](#)

[Close](#)

[Full Screen / Esc](#)

[Printer-friendly Version](#)

[Interactive Discussion](#)

